Dynamic behavior of an electron ring close to a cyclotron resonance in a modified betatron accelerator

D. Dialetis,* S. J. Marsh,† and C. A. Kapetanakos
Plasma Physics Division, Naval Research Laboratory, Washington, D.C. 20375-5000
(Received 15 June 1992)

The effect on the electron-ring dynamics when a cyclotron resonance is crossed in a modified betatron accelerator has been studied analytically and numerically. It has been found that, in the presence of small vertical field errors, there is a field-error-amplitude threshold below which the normalized transverse velocity $\beta_\perp$ of the gyrating electrons is bounded (Fresnel regime) and above which it is unbounded (lock-in regime). In the lock-in regime, the average value of the normalized axial (toroidal) momentum $\gamma\beta_\theta$, where γ is the relativistic factor and β_θ is the normalized axial velocity, remains constant, i.e., the resonance is never crossed. In addition, above threshold, $\beta_\perp$ increases proportionally to the square root of the time. The threshold value of the vertical field error amplitude can be made larger either by increasing the acceleration rate or by adding a small oscillatory toroidal field to the main toroidal field. The multiple crossing of the *same* resonance, in the presence of such a small oscillatory toroidal field, was also studied with some interesting results.

PACS number(s): 41.75.Fr, 41.85.Lc, 29.27.Bd

I. INTRODUCTION

There is extensive experimental evidence suggesting that the gradual beam loss that is observed in the Naval Research Laboratory (NRL) modified betatron accelerator (MBA) is a consequence of crossing various cyclotron resonance modes during acceleration [1,2]. The cyclotron resonance is due to the excitation of the cyclotron motion by field errors associated with the toroidal and vertical magnetic fields. Consequently, these field errors can be either a vertical-field δB_z (VF) error or an axial-(toroidal) field δB_θ (TF) error or both.

Recirculating accelerators with low accelerating gradient such as the existing NRL modified betatron are sensitive to field errors, because the electrons have to perform a large number of revolutions around the major axis in order to obtain the desired peak energy. Successful detection and elimination or reduction of several field errors in the NRL device led to beam energies in excess of 20 MeV, while the trapped current is above 1 kA [3].

Although the cyclotron resonance is a potent mechanism with the potential to disturb the beam at a low acceleration rate and when the various fields are not carefully designed, it also may provide a powerful technique for extracting the beam from the magnetic-field configuration of the modified betatron [4]. The study of the cyclotron resonances is facilitated by introducing the detuning factor $w = r_0\Omega_{\theta 0}/\gamma\beta_\theta c - l$, where r_0 is the major radius of the torus, c is the velocity of light, γ is the relativistic factor, β_θ is the normalized toroidal velocity, $\Omega_{\theta 0} = |e|B_{\theta 0}/mc$, $B_{\theta 0}$ is the toroidal magnetic field on the minor axis, e and m are the charge and mass of the electron, and l is the mode number of the resonance. The l mode of the cyclotron resonance occurs when the ratio of the toroidal field $B_{\theta 0}$ to the vertical field B_{z0} is approximately equal to l. Since at equilibrium the ratio $r_0\Omega_{z0}/\gamma\beta_\theta c$ is approximately unity, at least when the beam current is low and in the absence of strong focusing, the l-mode cyclotron resonance is crossed when the detuning factor is zero. Furthermore, the detuning factor appears naturally in the slow equations of motion derived by averaging out the fast cyclotron motion. The fact that $w + l$ is inversely proportional to $\gamma\beta_\theta$ has a profound effect on the ring dynamics. The quantity $\gamma\beta_\theta$ has a nonlinear dependence on the normalized perpendicular velocity $\beta_\perp$, and, as a consequence, there is a threshold for the vertical field error amplitude below which $\beta_\perp$ is bounded (Fresnel regime) and above which $\beta_\perp$ increases continuously (lock-in regime) with time. In the lock-in regime, the detuning factor remains almost zero long after the resonance has been reached and, therefore, the resonance is never crossed. In addition, above threshold, $\beta_\perp$ increases proportionally to the square root of time while $\gamma\beta_\theta$ remains, on the average, a constant. The threshold value of the vertical field error amplitude can be made larger either by increasing the acceleration rate or by adding a small oscillatory toroidal field to the main toroidal field. The latter method is called dynamic stabilization of the resonance.

In the case of a vertical field error and in the absence of acceleration, space charge, and strong focusing field, our studies of the cyclotron resonances show that the normalized transverse velocity $\beta_\perp$ and thus the Larmor radius of the transverse motion of the gyrating particles grows linearly with time [5], provided that nonlinear effects associated with $\gamma\beta_\theta$ are neglected. When such effects are taken into account, $\beta_\perp$ is periodic and bounded.

As mentioned previously, in the presence of an accelerating field and of a large vertical field error, $\beta_\perp$ increases proportionally to the square root of time while $\gamma\beta_\theta$ saturates, i.e., the electrons lock into a specific resonance (lock-in regime). When the amplitude of δB_z is

below the threshold, $\beta_\perp$ exhibits Fresnel behavior, i.e., $\beta_\perp$ grows quickly for approximately 1 μsec and then saturates until the beam reaches the next resonance.

In the case of an axial field error and in the absence of acceleration, when the ring is initially at exact resonance, $\beta_\perp$ grows exponentially with time only for a very short period. Since $\beta_\perp$ increases at the expense of β_θ, the particles are kicked off resonance and $\beta_\perp$ varies cyclicly with time. Similarly, in the presence of an accelerating field $\beta_\perp$ behaves as in the case of the vertical field error, i.e., below threshold it exhibits the Fresnel behavior and above threshold the ring locks into the resonance. The same is also true during acceleration even in the absence of a vertical or toroidal field error, but in the presence of stellarator fields of periodicity m, when the quasiequilibrium position of the ring is off the magnetic axis of the strong focusing system and the resonance mode is equal to m. The results of the studies with axial field error will be reported in a future publication. In the absence of a toroidal magnetic field, nonlinear effects associated with the crossing of resonances in synchrotrons have been considered previously by DePackh [6].

The preceding discussion is based on the assumption that the space charge is low and the strong focusing field is zero. In addition to introducing new characteristic modes, the strong focusing field makes the expression for the regular cyclotron mode more complicated [7]. However, it can be shown that for the parameters of the NRL device and provided $l \gg 1$, the strong focusing has only a minor effect on the cyclotron resonance. This conclusion is supported by extensive computer calculations.

This paper is organized as follows. The theoretical model is formulated in Sec. II. Section III A contains examples of both the Fresnel and lock-in state from the exact equations of motion. The slow equations of motion are derived in Sec. III B, and the simplified slow equations of motion with linearized detuning factor are given in Sec. III C. The asymptotic behavior in the Fresnel and lock-in state as well as the appropriate initial conditions to be used in the subsequent sections are presented in Sec. IV, while Sec. V contains a discussion of possible ways to cross a resonance without locking into it. Resonance diagrams for nonzero initial perpendicular velocity are displayed in Sec. VI, and the multiple crossing of the same resonance is demonstrated in Sec. VII. Finally, Sec. VIII contains the summary and conclusions.

II. MODEL WITH A VERTICAL-FIELD ERROR

Imperfections in the coils that generate the betatron field could result in a field error. A typical example is given in Fig. 1, which shows the VF error per kiloampere of the current circulating in the coils as a function of the toroidal angle, at $r=100$ cm. This error is due to a small straight section in each coil that generates the betatron field in the vicinity of the power feeds. Table I provides the Fourier decomposition of the error. The values are the actual error amplitudes (in G) for a toroidal field $B_{\theta 0}=4650$ G as each particular resonance is reached during acceleration.

Obviously, near a resonance, only the mode associated with that resonance is acting on the ring. The contribution of all the other modes, being far away from the resonance, averages out to zero due to their fast oscillatory behavior. Therefore the VF error will be expressed in terms of the particular l mode associated with the resonance under study, i.e.,

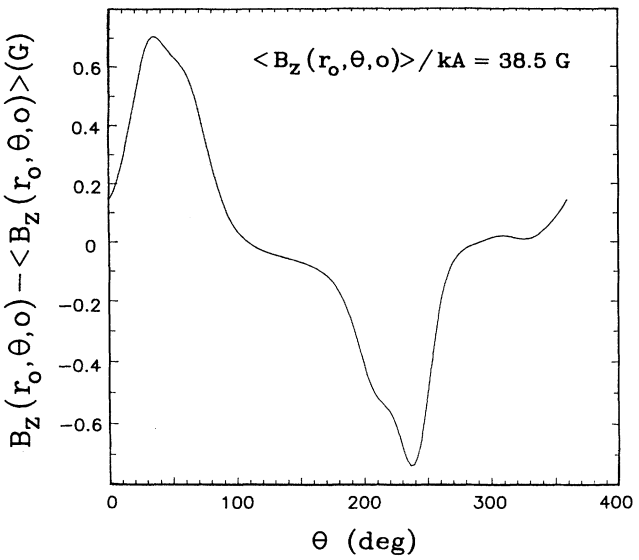

FIG. 1. Vertical field error per kiloampere of current in the coils that generate the betatron field, as a function of the toroidal angle θ, at $r=100$ cm, $z=0.0$ cm.

$$\delta B_r = \delta B_{z0} K_{r0} \frac{r-r_0}{r_0} \sin(l\theta+\theta_0) , \tag{1a}$$

$$\delta B_z = \delta B_{z0} \left[1+K_{r0}\frac{r-r_0}{r_0} \right] \sin(l\theta+\theta_0) , \tag{1b}$$

TABLE I. Fourier decomposition of VF error. Actual values of the VF error at each l mode for $B_\theta=4650$ G are listed.

Fourier mode	Fourier amplitude	cos (Fourier amplitude)	sin (Fourier amplitude)
1	108.2698	81.6151	71.1430
2	1.2152	0.3749	1.1559
3	8.8142	−6.5489	5.8994
4	0.9985	0.0905	0.9944
5	1.0148	−0.3835	−0.9395
6	0.5915	−0.5915	0.0000
7	0.3350	−0.0856	0.3238
8	0.3188	0.0884	−0.3063
9	0.3226	−0.2428	−0.2124
10	0.0759	0.0640	0.0407
11	0.1301	0.0868	−0.0970
12	0.0243	−0.0243	0.0000
13	0.0373	0.0264	0.0264
14	0.0112	0.0088	−0.0069
15	0.0062	−0.0045	0.0042
16	0.0034	0.0008	0.0033
17	0.0010	−0.0010	−0.0002
18	0.0012	−0.0012	0.0000
19	0.0002	−0.0002	0.0000
20	0.0000	0.0000	0.0000

$$\delta B_\theta = \delta B_{z0} \frac{z}{r_0} \cos(l\theta + \theta_0) \ . \tag{1c}$$

In Eqs. (1), δB_{z0}, θ_0, and K_{r0} are the amplitude, the phase, and the gradient in the radial direction of the l mode and r_0 is the major radius around which the analysis is carried out. It should be noticed that Eqs. (1a)–(1c) satisfy Maxwell's equations to first order in toroidal correlations.

The magnetic fields acting on the ring in the MBA are the betatron, the toroidal, and the stellarator field. For simplicity, the stellarator field is omitted in the present analysis. At high energies its contribution to the confinement of the ring is diminished and abundant computer runs have shown that the main results presented here are not altered in the presence of the stellarator field except for resonances $l = km$, where m is the field period of the stellarator and $k = 1, 2, \ldots$. In the analysis, the betatron field is approximated by

$$B_r^{(b)} = -nB_{z0} \frac{z}{r_0} \ , \tag{2a}$$

$$B_z^{(b)} = B_{z0} \left[1 - n \frac{r - r_0}{r_0} \right] \ , \tag{2b}$$

where n is the field index and B_{z0} the field on the minor axis. Similarly, the toroidal magnetic field is given by

$$B_\theta = B_{\theta 0} \frac{r_0}{r} \ , \tag{3}$$

where $B_{\theta 0}$ is the field at $r = r_0$.

Since the VF error is a sinusoidal function of the toroidal angle θ, it is convenient to express the equations of motion in terms of the independent variable θ rather than time. In their transformed state, the equations of motion become

$$\xi'' + \left[i \frac{r_0 \Omega_{\theta 0}}{\gamma \beta_\theta c} + \frac{1}{\gamma \beta_\theta} (\gamma \beta_\theta)' - \frac{1}{2} \frac{\xi' + \xi^{*\prime}}{1+P} \right] \xi' = i \frac{r_0 (\Omega_r + i\Omega_z)}{\gamma \beta_\theta c} (1+P)^2 + 1 + P \ , \tag{4}$$

where the complex variable $\xi = [(r - r_0) + iz]/r_0$, $\xi' = d\xi/d\theta$, ξ^* is the complex conjugate of ξ, and Ω is the cyclotron frequency, i.e., $\Omega = |e|B/mc$. The position of the ring centroid is given by

$$P \equiv \frac{r - r_0}{r_0} = \tfrac{1}{2}(\xi + \xi^*) \ , \tag{5a}$$

$$Q \equiv \frac{z}{r_0} = \frac{1}{2i}(\xi - \xi^*) \ . \tag{5b}$$

The quantity $\gamma\beta_\theta$ can be expressed as

$$\gamma \beta_\theta = \left[\frac{\gamma^2 - 1}{1 + \frac{1}{(1+P)^2} \xi' \xi^{*\prime}} \right]^{1/2} \ , \tag{6}$$

where γ is the relativistic factor and its derivative with respect to θ is equal to

$$\frac{1}{\gamma \beta_\theta} (\gamma \beta_\theta)' = \frac{\gamma \gamma'}{(\gamma \beta_\theta)^2} - \frac{r_0 \Omega_r}{\gamma \beta_\theta c} \frac{1}{2i} (\xi' - \xi^{*\prime}) - \left[1 - \frac{r_0 \Omega_z}{\gamma \beta_\theta c} (1+P) \right] \frac{1}{2} \frac{\xi' + \xi^{*\prime}}{1+P} \ . \tag{7}$$

The accelerating electric field is given by

$$E_\theta = -\frac{1}{c} r_0 \dot{B}_{z0} \ , \tag{8}$$

where $\dot{B}_{z0}$ is the time derivative of the betatron field at $r = r_0$. Using the rate of change of time that is given by $t' = (r_0/c\beta_\theta)(1+P)$, it can be shown that

$$\gamma' = \left[\frac{r_0}{c} \right]^2 \dot{\Omega}_{z0} (1+P) \tag{9}$$

and

$$\Omega'_{z0} = \frac{r_0}{c} \dot{\Omega}_{z0} \frac{\gamma}{\gamma \beta_\theta} (1+P) \ . \tag{10}$$

In the equations given above Ω_r and Ω_z include both the betatron field and the VF error. Notice that Eq. (4) is a second-order nonlinear differential equation of the complex quantity ξ. In terms of ξ, the position of the ring centroid is given by Eqs. (5), while its normalized velocity components v_r, v_z are

$$\beta_r + i\beta_z = \frac{\gamma \beta_\theta}{\gamma} \frac{1}{1+P} \xi' \ . \tag{11}$$

Obviously, the exact set of nonlinear equations given above is very complicated and difficult to handle. However, for a ring that has a bounce motion with a small amplitude, i.e., for small mismatch, and for large l-mode values, it is easy to show that near the resonance $|\xi| \approx |\xi'|/l$ and therefore $|\xi|$ is much smaller than $|\xi'|$. In this case, it is appropriate to linearize Eq. (4) with respect to ξ and ξ^*. Under such conditions, Eq. (4) simplifies to

$$\xi'' + ib\xi' + K_1 \xi = f_1 \ , \tag{12}$$

where

$$f_1 = \Delta + \left[\tfrac{1}{2}(1+\Delta)(\xi' + \xi^{*\prime}) + ib\zeta(\xi + \xi^*) - \frac{\gamma}{(\gamma\beta_\theta)_1^2} \gamma' - \tfrac{1}{2}(1 - nC)(\xi\xi' + \xi^*\xi^{*\prime}) - \tfrac{1}{2}(\xi^*\xi' + \xi\xi^{*\prime}) \right] \xi' - K_2 \xi^* + \zeta C(\xi + \xi^*) - \delta C[1 + \xi + (1 + K_{r0})\xi^* + \tfrac{1}{2}(\xi' + \xi^{*\prime})\xi'] \sin(l\theta + \theta_0) \ ,$$

$$\frac{1}{(\gamma\beta_\theta)_1} = \left[\frac{1 + \xi'\xi^{*\prime}}{\gamma^2 - 1} \right]^{1/2} \ , \tag{13a}$$

$$b=\frac{r_0\Omega_{\theta 0}}{(\gamma\beta_\theta)_1 c}\ , \tag{13b}$$

$$C=\frac{r_0\Omega_{z0}}{(\gamma\beta_\theta)_1 c}\ , \tag{13c}$$

$$\delta C=\frac{r_0\delta\Omega_{z0}}{(\gamma\beta_\theta)_1 c}\ , \tag{13d}$$

$$\zeta=\frac{1}{2}\frac{\xi'\xi^{*\prime}}{1+\xi'\xi^{*\prime}}\ , \tag{13e}$$

$$\Delta=1-C\ , \tag{13f}$$

$$K_1=C-\tfrac{1}{2}\ , \tag{13g}$$

$$K_2=(1-n)C-\tfrac{1}{2}\ . \tag{13h}$$

When the mismatch term Δ is small, then $C\approx 1$ and $K_2\approx\frac{1}{2}-n$. Since the term $K_2\xi^*$ in f_1 will be treated as a perturbation in the derivation of the slow equations of motion, K_2 must be small. Therefore we assume that n is close to $\frac{1}{2}$. Also, since we consider only values of $|\xi'|<0.2$, before the resonance is crossed, terms proportional to $|\xi'|^2|\xi|$ are omitted when compared to one. The simplified Eq. (12) is complemented by the derivatives with respect to θ of γ and $r_0\Omega_{z0}/c$, which are given by

$$\gamma'=\left[\frac{r_0}{c}\right]^2\dot{\Omega}_{z0}\left[1+\frac{\xi+\xi^*}{2}\right] \tag{14a}$$

and

$$\frac{r_0\Omega'_{z0}}{c}=\left[\frac{r_0}{c}\right]^2\dot{\Omega}_{z0}\frac{\gamma}{(\gamma\beta_\theta)_1}\left[1+\frac{\xi+\xi^*}{2}\right]\ . \tag{14b}$$

Results from the numerical integration of Eq. (12) and the exact Eq. (4) are in very good agreement, provided the initial values of $|\xi|<0.30\times10^{-2}$ and $|\xi'|<0.2$. Therefore Eq. (12) will be used in the derivation of the slow equations by averaging out the fast cyclotron oscillatory motion.

III. DYNAMIC BEHAVIOR NEAR A RESONANCE: FRESNEL AND LOCK-IN REGIMES

A. Numerical results from the exact equations

The results from the numerical integration of the exact equations of motion, i.e., Eq. (4), as a resonance is crossed during acceleration indicate the following consistent behavior: there is a threshold value of the VF error amplitude δB_{z0}, below which the perpendicular velocity $\beta_\perp$ of the gyrating electrons increases by a certain amount as the resonance is crossed and then it remains relatively constant, after the resonance has been crossed. Above the threshold value, $\beta_\perp$ keeps increasing with time while $\gamma\beta_\theta$ remains, on the average, constant, and the resonance is never crossed, i.e., the ring is locked into the resonance. A typical example of this behavior is shown in Fig. 2 for the parameters listed in Table II. The threshold value of δB_{z0} is between 0.19 and 0.195 G. Figures 2(a) and 2(c) show $\beta_\perp$ versus time below and above threshold, while Figs. 2(b) and 2(d) show the corresponding $\gamma\beta_\theta$ versus time.

It is rather difficult to find from the exact equations of motion the source of the dynamic behavior shown in Fig. 2. This behavior can be explained by the slow equations of motion derived in Sec. III B.

To derive the slow equations of motion the instantane-

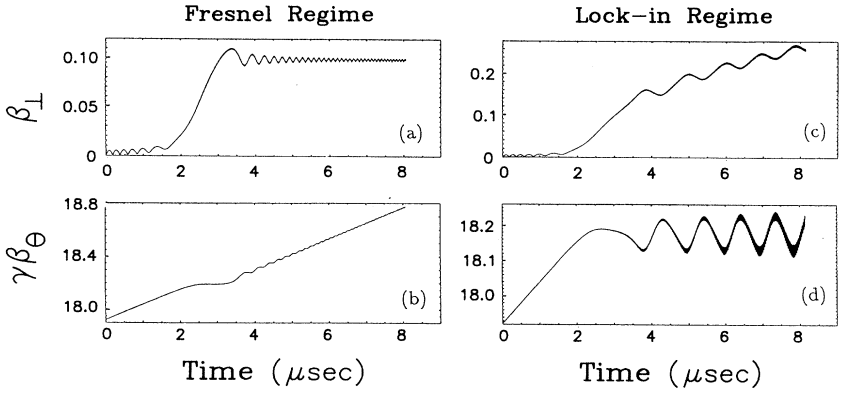

FIG. 2. $\beta_\perp$ and $\gamma\beta_\theta$ vs time obtained from the exact equations of motion [Eq. (4)], in the Fresnel and lock-in regimes and close to the threshold, for the parameters in Table II.

TABLE II. Parameters of the runs shown in Figs. 2–6.

Parameter	Value
Torus major radius r_0	100 cm
Toroidal magnetic field $B_{\theta 0}$	2771 G
Vertical magnetic field B_{z0}	305 G
Field index n	0.5
Rate of change of vertical field $\dot{B}_{z0}$	2 G/μsec
Resonance mode l	9
Amplitude of VF error δB_{z0}	0.190,0.195 G
Constant phase of VF error θ_0	0.0
Gradient of VF error K_{r0}	0.0
Initial normalized toroidal momentum $\gamma\beta_\theta$	17.922
Initial normalized vertical velocity $\beta_\perp$	0.0
Initial phase of vertical velocity φ_0	0.0
Initial radial displacement $r-r_0$	0.0 cm
Initial vertical displacement z	0.0 cm
Integration time t_f	8 μsec

ous position of the particle ξ is decomposed into two components. The first is associated with the bounce motion and the second with the cyclotron or fast motion, i.e., $\xi=\xi_b+\xi_c$, where $\xi_b=\xi_b^{(s)}\exp(-i\nu_b\theta)$, $\xi_c=\xi_c^{(s)}\exp(-i\nu_c\theta)$, and ν_b and ν_c are the two characteristic frequencies of the system. Specifically, $\nu_b=\nu_-$ and $\nu_c=\nu_+$, where

$$\nu_\pm=\frac{b}{2}\pm\left[\left[\frac{b}{2}\right]^2+K_1\right]^{1/2}. \tag{15}$$

The complex amplitudes $\xi_b^{(s)}$ and $\xi_c^{(s)}$ are, in general, slowly varying quantities, provided that the perturbation is not very large. Since these two amplitudes vary slowly, the corresponding derivatives with respect to θ are equal to $\xi_b'=-i\nu_b\xi_b$ and $\xi_c'=V_c^{(s)}\exp[-(l\theta+\theta_0)]$, provided that $\nu_c\simeq l$. The amplitude $V_c^{(s)}$ is a slowly varying quantity because ξ_c' has been expressed in a frame that rotates with angular velocity lc/r_0. As a consequence of $|V_c^{(s)'}|\ll|\xi'|$, the position of the cyclotron mode is given by $\xi_c\approx-(1/i\nu_c)V_c^{(s)}\exp[-i(l\theta+\theta_0)]$.

From the previous discussion, the complex position ξ and its derivative ξ' can be expressed as follows:

$$\xi=\xi_b-(1/i\nu_c)V_c^{(s)}e^{-i(l\theta+\theta_0)} \tag{16a}$$

and

$$\xi'=-i\nu_b\xi_b+V_c^{(s)}e^{-i(l\theta+\theta_0)}. \tag{16b}$$

It is apparent from Eqs. (16) that it is possible to extract the bounce and (slow) cyclotron motion in the rotating frame by inverting Eqs. (16). Specifically,

$$\xi_b=\frac{\nu_c}{\nu_c-\nu_b}\left[\xi-\frac{i}{\nu_c}\xi'\right] \tag{17a}$$

and

$$V_c^{(s)}=\frac{\nu_c}{\nu_c-\nu_b}(i\nu_b\xi+\xi')e^{i(l\theta+\theta_0)}. \tag{17b}$$

Figures 3(a) and 3(b) show the real and imaginary components of $\beta_\theta V_c^{(s)}$ for the parameters listed in Table II. For these same parameters, the actual orbit in the r-z plane, during the first 2 μsec, is given in Fig. 4(a), while Fig. 4(b) gives the bounce motion associated with the actual orbit, as computed from Eq. (17a).

B. Slow equations of motion

The method that is used in this section to obtain the equations of motion of the slowly varying quantities asso-

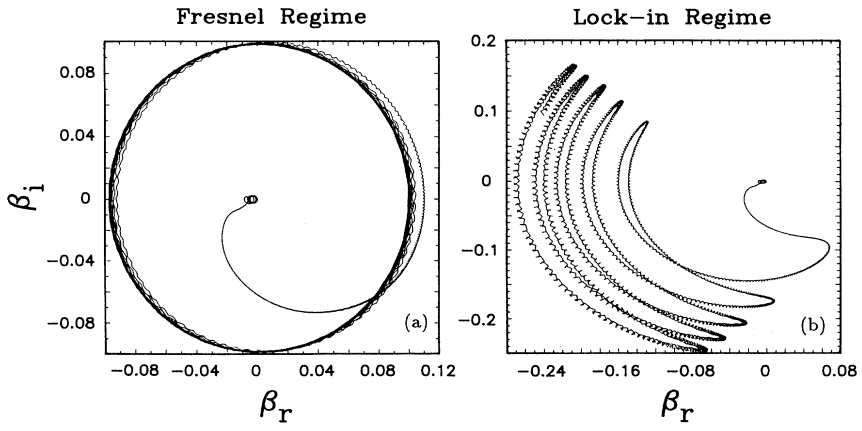

FIG. 3. Normalized perpendicular velocity in velocity space and in the rotating frame [Eq. (17b)] obtained from the exact equations of motion in the Fresnel and lock-in regimes (for the same parameters as in Fig. 2).

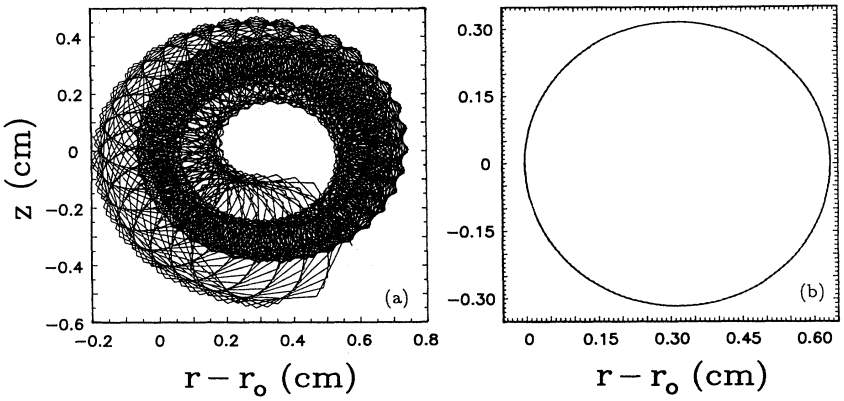

FIG. 4. (a) Exact orbit and (b) bounce motion orbit obtained from the exact equations of motion during the first 2 μsec, and for the same parameters as in Figs. 2 and 3.

ciated with the cyclotron and bounce motions has been devised by Bogoliubov and Mitropolsky [8] and is a perturbation approach to the problem. Before this method can be applied, the simplified Eq. (12) should be written in a suitable form. For this purpose we express ξ,ξ' in terms of the quantities ξ_b, V_c as follows:

$$\xi=\xi_b+\frac{i}{\nu_+}V_c\ , \tag{18a}$$

$$\xi'=-i\nu_-\xi_b+V_c\ , \tag{18b}$$

where

$$\nu_\pm=\frac{b_0}{2}\pm\left[\left[\frac{b_0}{2}\right]^2+K_{10}\right]^{1/2}\ , \tag{19a}$$

$$b_0=\frac{r_0\Omega_{\theta 0}}{(\gamma\beta_\theta)_0 c}\ , \tag{19b}$$

$$C_0=\frac{r_0\Omega_{z0}}{(\gamma\beta_\theta)_0 c}\ , \tag{19c}$$

$$K_{10}=C_0-\tfrac{1}{2}\ , \tag{19d}$$

$$\frac{1}{(\gamma\beta_\theta)_0}=\left[\frac{1+|V_0|^2}{\gamma^2-1}\right]^{1/2}\ , \tag{19e}$$

In Eq. (19e), V_0 is the zero order, slowly varying quantity associated with V_c [see Eq. (26a)]. In addition, $\nu_\pm$ are definitely slowly varying quantities, since they depend on $|V_0|^2$.

The equations of motion of V_c and ξ_b are

$$V_c'+i\nu_+V_c=\frac{\nu_+}{\nu_+-\nu_-}\left[f+\delta f+i\nu_-'\xi_b-\frac{\nu_+'}{\nu_+}\frac{\nu_-}{\nu_+}V_c\right]\ , \tag{20a}$$

$$\xi_b'+i\nu_-\xi_b=-\frac{i}{\nu_+-\nu_-}\left[f+\delta f+i\nu_-'\xi_b-\frac{\nu_+'}{\nu_+}V_c\right]\ , \tag{20b}$$

where

$$f=\Delta_0+\tfrac{1}{2}(1+\Delta_0)(\xi'+\xi^{*\prime})\xi'-\delta C_0\sin(l\theta+\theta_0)\ , \tag{21a}$$

$$\delta f=\Delta-\Delta_0+\left[-i(b-b_0)+\tfrac{1}{2}(\Delta-\Delta_0)(\xi'+\xi^{*\prime})+ib\zeta(\xi+\xi^*)-\frac{\gamma}{(\gamma\beta_\theta)_1^2}\gamma'\right.$$
$$\left.-\tfrac{1}{2}(1-nC)(\xi\xi'+\xi^*\xi^{*\prime})-\tfrac{1}{2}(\xi^*\xi'+\xi\xi^{*\prime})\right]\xi'-(K_1-K_{10})\xi-K_2\xi^*+\zeta C(\xi+\xi^*)$$
$$-\delta C[\xi+(1+K_{r0})\xi^*+\tfrac{1}{2}(\xi'+\xi^{*\prime})\xi']\sin(l\theta+\theta_0)-(\delta C-\delta C_0)\sin(l\theta+\theta_0)\ . \tag{21b}$$

$$\Delta_0=1-C_0\ , \tag{22a}$$

$$\delta C_0=\frac{r_0\delta\Omega_{z0}}{(\gamma\beta_\theta)_0 c}\ , \tag{22b}$$

and b_0, C_0, K_{10} have already been defined.

To implement the perturbation theory, we introduce the parameter ϵ, which indicates the relative smallness of the various terms. In terms of ϵ, Eqs. (20) can be written as follows:

$$V_c'+ilV_c=\epsilon[f_c-i(\nu_+-l)V_c]\ , \tag{23a}$$

$$\xi_b'+i\epsilon\nu_-\xi_b=\epsilon f_b\ , \tag{23b}$$

where

$$f_c=\frac{\nu_+}{\nu_+-\nu_-}[f+\delta f]\ , \tag{24a}$$

$$f_b=-\frac{i}{\nu_+-\nu_-}[f+\delta f]\ . \tag{24b}$$

Assuming that the field error $\delta B_{z0}\ll B_{z0}$, $|\Delta_0|\ll 1$, and since $l\gg|V_0|$ and $\nu_+\approx l$, the right-hand side of Eqs. (23) is at least of order ϵ. In addition, since $|\nu_-|\ll 1$, the term $i\nu_-\xi_b$ in Eq. (23b) is of order ϵ. The terms that are proportional to the derivatives of $\nu_\pm$ have been omitted because they are of higher order.

Furthermore, for high l-mode numbers $|\xi|\ll|\xi'|$ and in light of Eqs. (18), in terms of ϵ, ξ and ξ' can be written as follows:

$$\xi=\epsilon\left[\xi_b+\frac{i}{\nu_+}V_c\right]\ , \tag{25a}$$

$$\xi'=-i\nu_-\xi_b\epsilon+V_c\ . \tag{25b}$$

The perturbation method is applied on Eqs. (23) and (25) by setting

$$V_c=V_0e^{-i(l\theta+\theta_0)}+\epsilon V_1(\xi_0,\xi_0^*,V_0,V_0^*,\theta)+\cdots\ , \tag{26a}$$

$$\xi_b=\xi_0+\epsilon\xi_1(\xi_0,\xi_0^*,V_0V_0^*,\theta)+\cdots\ , \tag{26b}$$

$$V_0'=\epsilon A_1(\xi_0,\xi_0^*,V_0,V_0^*)+\epsilon^2A_2(\xi_0,\xi_0^*,V_0,V_0^*)+\cdots\ , \tag{26c}$$

$$\xi_0'=\epsilon B_1(\xi_0,\xi_0^*,V_0,V_0^*)+\epsilon^2B_2(\xi_0,\xi_0^*,V_0,V_0^*)+\cdots\ , \tag{26d}$$

where V_0,ξ_0 are the slowly varying quantities associated with V_c,ξ_b, respectively. Then, the slowly varying quantities $A_1,A_2,\ldots$ and $B_1,B_2,\ldots$ are determined by inserting the equations above into Eqs. (23) and eliminating the terms that lead to secular terms for each order of the perturbation parameter ϵ.

The computation is carried out to second order in ϵ and it is tedious but straightforward and will not be given here. To that order, the quantities V_1,ξ_1, are equal to

$$V_1=\frac{\nu_+}{\nu_+-\nu_-}\frac{1}{il}\left[\Delta_0+\tfrac{1}{2}(1+\Delta_0)|V_0|^2+\frac{i}{4}\delta C_0e^{i(l\theta+\theta_0)}-\tfrac{1}{2}(1+\Delta_0)V_0^2e^{-2i(l\theta+\theta_0)}\right]\ , \tag{27a}$$

$$\xi_1=-\frac{i}{\nu_+-\nu_-}\frac{1}{2l}\left[\delta C_0e^{-i(l\theta+\theta_0)}+\delta C_0e^{i(l\theta+\theta_0)}+\frac{i}{2}(1+\Delta_0)V_0^2e^{-2i(l\theta+\theta_0)}\right]\ . \tag{27b}$$

Also, to second order in ϵ, the slow equations for V_0 and ξ_0 are

$$V_0'+i(\nu_+-l)V_0=f_c^{(s)}\ . \tag{28a}$$

and

$$\xi_0'+i\nu_-\xi_0=f_b^{(s)}\ , \tag{28b}$$

where

$$f_c^{(s)}=i\frac{\nu_+}{\nu_+-\nu_-}\left\{i\frac{\gamma\gamma'}{(\gamma\beta_\theta)_0^2}V_0-\nu_-\xi_0V_0+b_0\xi_0(\xi_0+\xi_0^*)V_0-\left[\Delta_0+\frac{\xi_0C_0}{2}\right]\nu_-(\xi_0-\xi_0^*)V_0+\frac{C_0}{2\nu_+}[\xi_0(1-|V_0|^2)-\Delta_0(1+2\xi_0-\Delta_0(1+\tfrac{3}{2}|V_0|^2))]V_0-\frac{\delta C_0}{2}\left[1+\xi_0+(1+K_{r0})\xi_0^*+\tfrac{1}{2}|V_0|^2-\tfrac{1}{2}V_0^2-\frac{\delta C_0}{8\nu_+}\frac{1}{1+|V_0|^2}V_0\right]\right\}\ , \tag{29a}$$

and

$$f_b^{(s)}=-\frac{i}{\nu_+-\nu_-}\left\{\Delta_0+\tfrac{1}{2}|V_0|^2-(b_0\nu_-+\Delta_0+|V_0|^2)\xi_0\xi_0-\left[K_{20}-\frac{nC_0}{2}|V_0|^2+(\Delta_0+|V_0|^2)\xi_0\right]\xi_0^*-\frac{\delta C_0}{2\nu_+}\left[\left[1+\tfrac{1}{2}\Delta_0+\xi_0-\frac{1}{2}\frac{K_{10}\xi_0}{1+|V_0|^2}\right](V_0+V_0^*)+K_{r0}V_0^*-\frac{\delta C_0}{4}\xi_0V_0\right]\right\}\ . \tag{29b}$$

The quantities for ξ_0 and K_{20} are given in Eqs. (13e) and (13h) with $|\xi'|^2$ replaced by $|V_0|^2$ and C replaced by C_0. The slow Eqs. (28) and (29) should be complemented by the derivatives of γ and $r_0\Omega_{z0}/c$. Keeping only the zero order nonoscillatory parts in Eqs. (14a) and (14b), we obtain

$$\gamma'\approx\left[\frac{r_0}{c}\right]^2\dot{\Omega}_{z0}\left[1+\frac{\xi_0+\xi_0^*}{2}\right] \tag{30}$$

and

$$\frac{r_0\Omega_{z0}'}{c}\approx\left[\frac{r_0}{c}\right]^2\dot{\Omega}_{z0}\frac{\gamma}{(\gamma\beta_\theta)_0}\left[1+\frac{\xi_0+\xi_0^*}{2}\right]\ . \tag{31}$$

Solutions of the slow equations are shown in Fig. 5 for the same input parameters (see Table II) used in the solution of the exact Eq. (4). Figures 5(a) and 5(c) show the zero order $\beta_\perp^{(0)}\equiv(\gamma\beta_\theta)_0|V_0|/\gamma$ versus time, below and

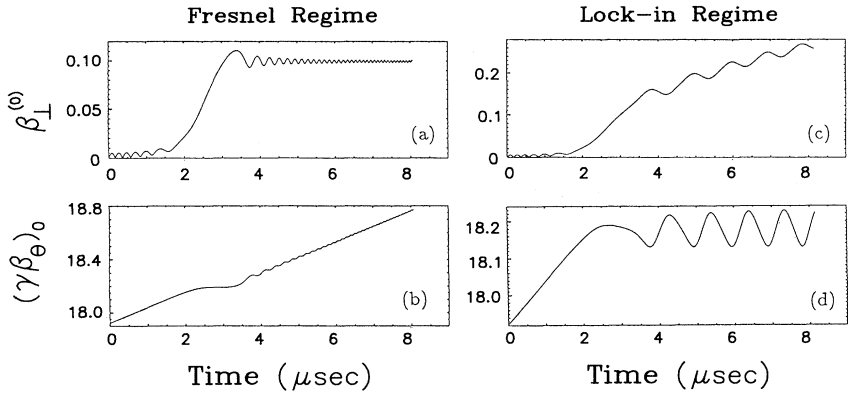

FIG. 5. $\beta_\perp$ and $\gamma\beta_\theta$ vs time obtained from the slow equations of motion [Eqs. (28) and (29)], in the Fresnel and lock-in regimes and close to the threshold, for the parameters in Table II.

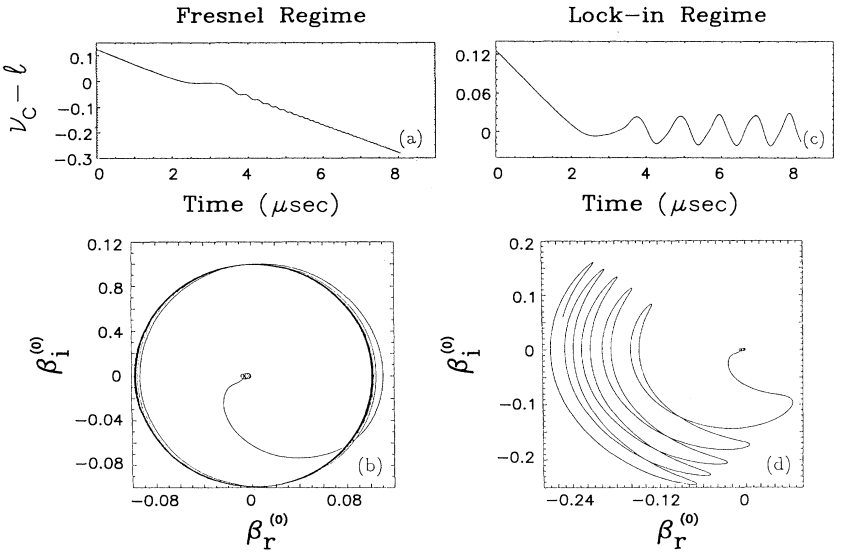

FIG. 6. Detuning factor vs time and normalized perpendicular velocity in velocity space obtained from the slow equations of motion in the Fresnel and lock-in regimes (for the same parameters as in Fig. 5).

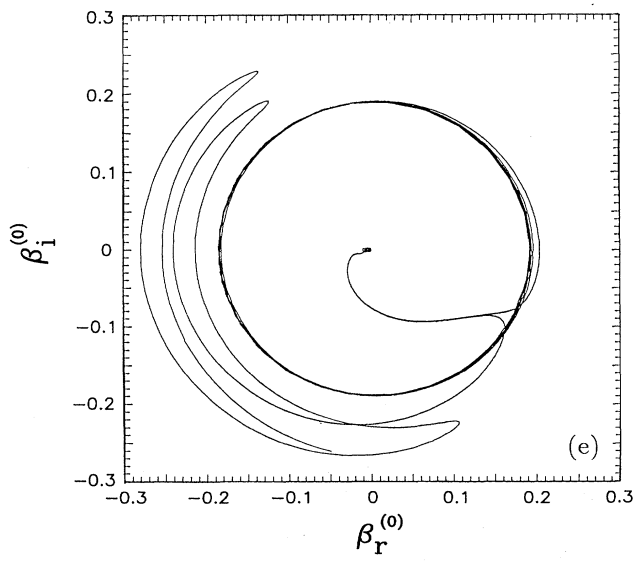

above threshold, while Figs. 5(b) and 5(d) show the corresponding zero order $(\gamma\beta_\theta)_0$ versus time. Figure 6 shows the detuning factor $w=\nu_c-l$ and the real and imaginary parts of $(\gamma\beta_\theta)_0 V_0/\gamma$, below and above threshold. By comparing Figs. 5 and 6 to Figs. 2 and 3 it is apparent that the slow equations predict accurately $\beta_\perp$ and $\gamma\beta_\theta$, when the initial perpendicular velocity is zero. Above threshold the detuning factor locks into the resonance, with only a small variation around zero. A plot of ξ_0 is not given, since it is exactly the same as that in Fig. 4(b). Obviously, the numerical integration of the slow equations is much faster than that of the exact Eq. (4) or (12), since the oscillatory terms have been averaged out.

C. Slow equations of motion with linearized detuning factor

The slow equations of Sec. III B are still too lengthy to provide insight into the origin of the threshold behavior. When $\delta B_{z0}|V_0|/lB_{z0}\ll 1$, the last term in Eq. (29b) can be neglected and the equation for the bounce motion simplifies to the equation

$$\xi_0'+i\nu_-\left[1+\frac{1}{K_{10}}(b_0\nu_-+\Delta_0+|V_0|^2)\right]\xi_0 +i\frac{\nu_-}{K_{10}}\left[K_{20}-\frac{nC_0}{2}|V_0|^2+(\Delta_0+|V_0|^2)\xi_0\right]\xi_0^* =i\frac{\nu_-}{K_{10}}(\Delta_0+\tfrac{1}{2}|V_0|^2)\ , \quad (32)$$

where we have used the fact that $|\nu_-|\ll\nu_+$, and the relation $\nu_-\nu_+=-K_{10}$. Equation (32) indicates that the equilibrium position of the bounce motion is proportional to the generalized mismatch $\Delta_0+\frac{1}{2}|V_0|^2$. Without exception the computer runs have shown that during the crossing of the resonance the equilibrium position of the bounce motion hardly changes when the gradient factor $K_{r0}=0$. That is not the case when $K_{r0}\neq 0$. Therefore, if both the initial mismatch and the initial bounce position ξ_0 are zero, the latter quantity remains very small. Under these conditions, the slow equation for V_0 simplifies to the equation

$$V_0'+i\left[\nu_+-l+\frac{C_0}{2\nu_+}(\Delta_0-\tfrac{1}{2}|V_0|^2)\right]V_0 =i\left[i\frac{\gamma\gamma'}{(\gamma\beta_\theta)_0^2}V_0-\frac{\delta C_0}{2}(1+\tfrac{1}{2}|V_0|^2-\tfrac{1}{2}V_0^2)\right]\ , \quad (33)$$

where terms proportional to Δ_0^2, $|V_0|^4$, and $\Delta_0|V_0|^2$ or higher have been omitted.

To simplify further Eq. (33), it is convenient to introduce the quantity U_0 by means of the relation

$$V_0=\frac{U_0}{[\gamma^2-1-|U_0|^2]^{1/2}}\ . \quad (34)$$

Since, to zero order, V_0 is equal to $[(\beta_r+i\beta_z)/\beta_\theta]\exp[i(l\theta+\theta_0)]$, U_0 is, to the same order, equal to $\gamma(\beta_r+i\beta_z)\exp[i(l\theta+\theta_0)]$, and it is easy to show from Eqs. (19e) and (34) that

$$(\gamma\beta_\theta)_0=[\gamma^2-1-|U_0|^2]^{1/2}\ . \quad (35)$$

A straightforward transformation of Eq. (33) from the V_0 to the U_0 variable leads to the slow equation for U_0, namely

$$U_0'+i\left[\nu_+-l+\frac{C_0}{2\nu_+}\left[\Delta_0-\frac{1}{2}\frac{|U_0|^2}{(\gamma\beta_\theta)_0^2}\right]\right]U_0=-iB_0\ , \quad (36)$$

where

$$B_0=\frac{1}{2}\frac{r_0\delta\Omega_{z0}}{c}\ . \quad (37)$$

Equation (36) indicates that the detuning factor $w=\nu_+-l$ should be redefined by adding to it the small correction term

$$C_0\left[\Delta_0-\frac{1}{2}\frac{|U_0|^2}{(\gamma\beta_\theta)_0^2}\right]\Big/2\nu_+\ .$$

Above threshold, the small correction term is important because it compensates for the small time-dependent contribution of K_{10} in ν_+ [cf. Eq. (19a)]. If the small correction term is omitted in either Eq. (36) or (33), then, above threshold, the average value of $(\gamma\beta_\theta)_0$ does not remain constant but increases with θ. This is contrary to the solution of either Eqs. (28) and (29) or the exact Eq. (4) or (12).

When the mismatch $\Delta_0+\frac{1}{2}|V_0|^2\approx 0$ and the initial ξ_0 is also zero, then $\xi_0\approx 0$ and the relativistic factor γ is equal to $\gamma=\gamma_0+\gamma'\theta$ [cf. Eq. (30)], where γ_0 and γ' are the initial values of γ and the acceleration rate [assumed to be a constant, and given by Eq. (30) with $\xi_0=0$], respectively. Assuming that $\gamma'\theta\ll\gamma_0$ and $||U_0|^2-|U_{00}|^2|\ll 1$, where U_{00} is the initial value of U_0, the detuning factor can be linearized with respect to $\gamma'\theta$ and $|U_0|^2-|U_{00}|^2$, namely

$$w=w_0-\alpha\theta+\tfrac{1}{2}\delta[|U_0|^2-|U_{00}|^2]\ , \quad (38)$$

where

$$w_0=\nu_{+0}-l+\frac{C_{00}}{2\nu_{+0}}\left[\Delta_{00}-\frac{1}{2}\frac{|U_{00}|^2}{(\gamma\beta_\theta)_{00}^2}\right]\ , \quad (39a)$$

$$\alpha=\nu_{+1}\frac{\gamma_0\gamma'}{(\gamma\beta_\theta)_{00}^2}\ , \quad (39b)$$

$$\delta=\nu_{+1}\frac{1}{(\gamma\beta_\theta)_{00}^2}\ , \quad (39c)$$

$$\nu_{+1}=\frac{b_{00}}{2}\left[1+\frac{\frac{b_{00}}{2}}{\left[\left[\frac{b_{00}}{2}\right]^2+K_{100}\right]^{1/2}}\right]\ , \quad (39d)$$

$$(\gamma\beta_\theta)_{00}=[\gamma_0^2-1-|U_{00}|^2]^{1/2}\ , \quad (39e)$$

and $\nu_{+0},b_{00},c_{00},\Delta_{00},K_{100}$ are the initial values of $\nu_+,b_0,c_0,\Delta_0,K_{10}$, respectively. The dependence of K_{10}

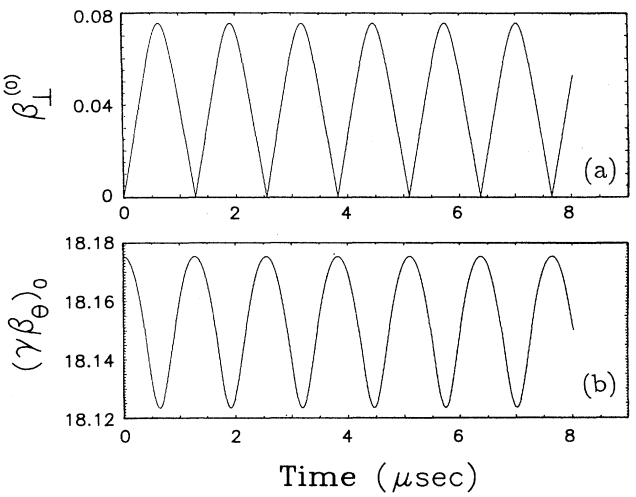

FIG. 7. $\beta_\perp$ and $\gamma\beta_\theta$ vs time obtained from the slow equations of motion without acceleration, for the parameters in Table III.

on θ and on $(\gamma\beta_\theta)_0$ has been neglected, since ν_+ is weakly dependent on K_{10} when $b_0 \approx l \gg 1$. Also, since $\Delta_0 \approx -\frac{1}{2}|U_0|^2/(\gamma\beta_\theta)_0^2$, $C_0 \approx 1$, and $\delta \approx l/(\gamma\beta_\theta)_{00}^2$, the small correction term that is added to the detuning factor in Eq. (36) provides such a small contribution to δ, of order $1/l^2$, that it has been neglected. Therefore the slow equation for U_0 with linearized detuning factor is

$$U_0' + i[w_0 - \alpha\theta + \tfrac{1}{2}\delta(|U_0|^2 - |U_{00}|^2)]U_0 = -iB_0 \ . \tag{40}$$

This equation predicts the same temporal behavior for $\beta_\perp$ and $\gamma\beta_\theta$ as the original slow Eqs. (28) and (29). The cause of this behavior is the nonlinear term proportional to $|U_0|^2 - |U_{00}|^2$ (it will be shown shortly that when $\delta = 0$, the solution is the Fresnel integral, which is bounded). We conclude that the existence of the Fresnel and lock-in regimes in the exact Eq. (4) or in Eq. (12) is due to the dependence of the term $r_0\Omega_{\theta 0}/\gamma\beta_\theta c$ upon $\gamma\beta_\theta$ and the fact that $\gamma\beta_\theta$ depends nonlinearly on the perpendicular velocity.

It is interesting to examine the case when there is no acceleration ($\alpha = 0$), the particles are at exact resonance ($w_0 = 0$) and the initial perpendicular velocity is zero ($|U_{00}|^2 = 0$). Then Eq. (40) becomes

$$U_0' + i\tfrac{1}{2}\delta|U_0|^2 U_0 = -iB_0 \ , \tag{41}$$

and it can be solved exactly. For that purpose, define $A \equiv |U_0|^2$. Then, separating the real and imaginary parts of Eq. (41), it is easy to show that

$$U_{0r} = -\frac{\delta}{8B_0} A^2 \ , \tag{42a}$$

$$U_{0i} = -\frac{1}{2B_0} A' \ , \tag{42b}$$

and from the definition of A it follows that

$$A' = \left[A \left[4B_0^2 - \frac{\delta^2}{16} A^3 \right] \right]^{1/2} . \tag{43}$$

The exact solution of this differential equation is

$$\int_0^{\lambda^2 A} \frac{dx}{[x(1-x)(x^2+x+1)]^{1/2}} = 2B_0\lambda\theta \ , \tag{44}$$

where $\lambda = (\delta/8B_0)^{1/3}$. The integral can also be expressed in terms of the elliptic integral of the first kind [9] $F(\varphi, k)$, i.e.,

$$F\left[2\,\mathrm{arccot}\frac{1}{3^{1/4}} \left[\frac{1-\lambda^2 A}{\lambda^2 A} \right]^{1/2}, \frac{\sqrt{2-\sqrt{3}}}{2} \right] = 3^{1/4} 2B_0\lambda\theta \ . \tag{45}$$

For very small or very large values of the argument of the arccot, the approximate solution is

$$A \equiv (\gamma_0\beta_\perp)^2 = \left[\frac{8B_0}{\delta} \right]^{2/3} \frac{\tan^2\mu\theta}{\sqrt{3} + \tan^2\mu\theta} \ , \tag{46}$$

where $\mu = 3^{1/4}\lambda B_0$. The solution of Eq. (43) is bounded. When $\mu\theta \ll 1$, $A \approx (B_0\theta)^2$ and $\beta_\perp$ is proportional to θ, which is the usual linear secular solution. But the nonlinear dependence of $\gamma\beta_\theta$ on $\beta_\perp$ forces the solution to be bounded. Figure 7 shows $\beta_\perp$ and $\gamma\beta_\theta$ versus time for the parameters listed in Table III, by integrating either the

TABLE III. Parameters of the run shown in Fig. 7.

Parameter	Value
Torus major radius r_0	100 cm
Toroidal magnetic field $B_{\theta 0}$	2771 G
Initial generalized mismatch $\Delta_0 + 0.5\|V_0\|^2$	0.0
Field index n	0.5
Rate of change of vertical field $\dot{B}_{z0}$	0.0 G/μsec
Resonance mode l	9
Amplitude of VF error δB_{z0}	0.3 G
Constant phase of VF error θ_0	0.0
Gradient of VF error K_{r0}	0.0
Initial normalized toroidal momentum $\gamma\beta_\theta$	18.1753
Initial normalized vertical velocity $\beta_\perp$	0.0
Initial phase of vertical velocity φ_0	0.0
Initial normalized radial bounce displacement ξ_{0x}	0.0
Initial normalized vertical bounce displacement ξ_{0z}	0.0
Integration time t_f	8 μsec

slow Eq. (40) or (36), or Eqs. (28) and (29). Integration of the exact Eq. (4) for the same parameters also gives identical results. The peak value of $\beta_\perp$ and the period $(\pi/\mu)r_0/c$ as computed from the approximate Eq. (46) are 0.0757 and 1.247 μsec, respectively, in good agreement with Fig. 7.

In conclusion, our analysis indicates that there is a completely different behavior near a resonance with or without acceleration. Even at exact resonance, $\beta_\perp$ is always bounded without acceleration, but it is unbounded with acceleration and in the presence of a large field error.

IV. ASYMPTOTIC BEHAVIOR IN THE FRESNEL AND LOCK-IN REGIMES

In order to study the asymptotic behavior of Eq. (40), it is convenient to transform it into dimensionless form. For this purpose, when $\alpha>0$, we introduce the quantities $\sigma=\sqrt{\alpha}\theta$, $\sigma_0=w_0\sqrt{\alpha}$, $\hat{\epsilon}=(\delta/2\alpha^{3/2})^{1/2}B_0$, and $\hat{U}_0=(\delta/2\alpha^{1/2})U_0$.

Then, Eq. (40) becomes

$$\frac{d\hat{U}_0}{d\sigma}+i[\sigma_0-\sigma+|\hat{U}_0|^2-|\hat{\tilde{U}}_{00}|^2]\hat{U}_0=-i\hat{\epsilon}\ , \tag{47}$$

where $\hat{\tilde{U}}_{00}$ is not equal to the initial value of $\hat{U}_0$ and will be defined shortly. Let $\hat{\epsilon}_{\rm thr}$ be the threshold value of $\hat{\epsilon}$. When $\hat{\epsilon}\ll\hat{\epsilon}_{\rm thr}$, i.e., when $B_0^2\delta/(2\alpha^{3/2})\ll\hat{\epsilon}_{\rm thr}^2$, the change in $\hat{U}_0$ associated with the crossing of the resonance is small, i.e., $||\hat{U}_0|^2-|\hat{\tilde{U}}_{00}|^2|\ll 1$, and Eq. (47) simplifies to

$$\frac{d\hat{U}_0}{d\sigma}+i(\sigma_0-\sigma)\hat{U}_0=-i\hat{\epsilon}\ . \tag{48}$$

The crossing of the resonance occurs at $\sigma=\sigma_0$, i.e., at $\theta_0=w_0/\alpha$. The solution of this equation is

$$\hat{U}_0=e^{i(1/2)(\sigma-\sigma_0)^2}\left[\hat{U}_{00}e^{-i(1/2)\sigma_0^2}-i\hat{\epsilon}\int_{-\sigma_0}^{\sigma-\sigma_0}e^{-i(1/2)\sigma'^2}d\sigma'\right]\ , \tag{49}$$

i.e., the particular solution can be written in terms of the Fresnel integral. When $\sigma_0\gg 1$, the asymptotic expression of the Fresnel integral leads to the approximate solution

$$U_0\approx e^{i(w^2/2\alpha)}\left[\left[U_{00}+\frac{B_0}{w_0}\right]e^{-i(w_0^2/2\alpha)}-i\frac{B_0}{\sqrt{\alpha}}\int_{-\infty}^{-w/\sqrt{\alpha}}e^{-i(1/2)\xi'^2}d\xi'\right]\ , \tag{50}$$

where the solution has been transformed to the original variables and $w=w_0-\alpha\theta$. U_0 is very sensitive to the phase $w_0^2/2\alpha$, when $U_{00}+B_0/w_0\neq 0$. Since $\alpha\ll 1$, a small change in the initial time interval $\tau_0\equiv(r_0/c)w_0/\alpha$ from the resonance [e.g., a small change in the initial value of $(\gamma\beta_\theta)_0$] will cause a very different behavior of $|U_0|$ versus time. To alleviate this problem, we define the initial condition of Eq. (50), and also of Eq. (40), by means of the initial variable $\tilde{U}_{00}$, i.e.,

$$U_{00}=\tilde{U}_{00}e^{i(w_0^2/2\alpha)}-\frac{B_0}{w_0}\ , \tag{51}$$

where $\tilde{U}_{00}=(\delta/2\alpha^{1/2})^{-1}\hat{\tilde{U}}_{00}$ and $\hat{\tilde{U}}_{00}$ is the value in Eq. (47) around which the detuning factor is linearized. Then Eq. (50) becomes

$$U_0=e^{i(w^2/2\alpha)}\left[\tilde{U}_{00}-i\frac{B_0}{\sqrt{\alpha}}\int_{-\infty}^{-w/\sqrt{\alpha}}e^{-i(1/2)\xi'^2}d\xi'\right]\ , \tag{52}$$

and is independent of τ_0, but it does depend on the initial phase of $\tilde{U}_{00}$. Equation (52) indicates that as θ tends to minus infinity, $||U_0|^2-|\tilde{U}_{00}|^2|$ tends to zero. Therefore $|\tilde{U}_{00}|$ is the appropriate constant around which the detuning factor should be linearized, and w_0,α,δ become functions of $\tilde{U}_{00}$ (and not of U_{00}). Because $|U_0|$ tends to $|\tilde{U}_{00}|$ as $\theta\to-\infty$ we shall call $\tilde{U}_{00}$ the asymptotic initial value of U_0. When $\theta\gg 1$ (or $|w|/\sqrt{\alpha}\gg 1$), the asymptotic value of $|U_0|$ is

$$|U_0|\sim|\tilde{U}_{00}-iB_0\sqrt{\pi/\alpha}(1+i)|\ . \tag{53}$$

Therefore, when $\tilde{U}_{00}\neq 0$, the final value of $|U_0|$ could be smaller than its asymptotic initial value $|\tilde{U}_{00}|$. When $\tilde{U}_{00}=0$, the asymptotic value of $\beta_\perp$ is

$$\beta_\perp(\theta\gg 1)=\sqrt{2\pi/\alpha}\frac{B_0}{\gamma_0+\gamma'\theta}\ , \tag{54}$$

where $|\gamma'\theta|\ll\gamma_0$. Since the width of the Fresnel integral is $\Delta\sigma=2\pi^{1/2}$, we conclude that the time Δt it takes for the resonance to be crossed is

$$\Delta t=2\frac{r_0}{c}\sqrt{\pi/\alpha}\ . \tag{55}$$

Therefore the final $\beta_\perp$ and Δt are inversely proportional to the square root of the acceleration rate in the Fresnel regime, provided $\hat{\epsilon}\ll\hat{\epsilon}_{\rm thr}$. Figure 8 shows $\beta_\perp^{(0)}$ and $(\gamma\beta_\theta)_0$ versus time for the parameters of Table II, except that $\delta B_{z0}=0.1$ G, i.e., far away from the threshold. Notice the smooth variation of $\beta_\perp^{(0)}$ during the first microsecond and compare to the oscillatory behavior that occurs in Fig. 5(a). The difference is due to the choice of the initial condition. In Fig. 8(a), $\tilde{U}_{00}=0$, while in Fig. 5(a), $U_{00}=0$. When $w>0$ and $|w|/\sqrt{\alpha}\gg 1$, i.e., well before the resonance crossing, the asymptotic value of U_0, as given by Eq. (52), is

$$U_0\sim\tilde{U}_{00}e^{i(w^2/2\alpha)}-\frac{B_0}{w}\ . \tag{56}$$

When $\tilde{U}_{00}=0$, we have $|U_0|=-B_0/|w|$, which explains the smooth variation of $\beta_\perp^{(0)}$ in Fig. 8(a).

We have shown above that if the initial condition, given by Eq. (51), is chosen the solution of Eq. (40), in either the Fresnel or the lock-in regime, is independent of the initial time interval τ_0 from the resonance, when $w_0/\sqrt{\alpha}\gg 1$. This is no longer true if the initial condition given by Eq. (51) is chosen for the solution of Eq.

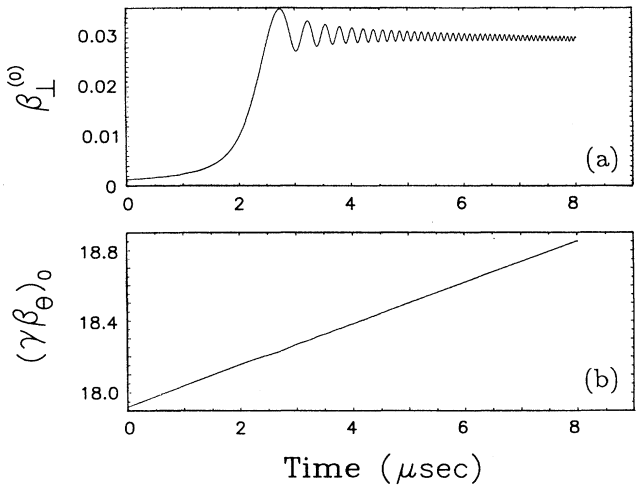

FIG. 8. $\beta_\perp$ and $\gamma\beta_\theta$ vs time from the slow equations of motion in the Fresnel regime far away from the threshold, i.e., for the parameters of Table II, except that $\delta B_{z0}=0.1$ G [the initial condition is given by Eq. (51), with $\tilde{U}_{00}=0$].

(36), which has a nonlinear detuning factor w. The nonlinear dependence of w on θ causes the solution to depend on τ_0. To second order in θ, the detuning factor is given by

$$w=w_0-\alpha\theta+\tfrac{1}{2}\alpha_2\theta^2+\tfrac{1}{2}\delta[|U_0|^2-|\tilde{U}_{00}|^2]\ , \tag{57}$$

where w_0,α,δ have already been defined, $\tilde{U}_{00}$ will be redefined shortly, and

$$\alpha_2=\left[3-\frac{(\gamma\beta_\theta)_{00}^2}{\gamma_0^2}\right]\frac{\gamma_0\gamma'}{(\gamma\beta_\theta)_{00}^2}\alpha\ . \tag{58}$$

When $w/\sqrt{\alpha}\gg 1$, i.e., well before the resonance crossing, the term proportional to δ can be neglected in Eq. (57), and the asymptotic solution of Eq. (40) is

$$U_0\sim\exp\left[-i\int_0^\theta w\,d\theta\right]\left[U_{00}+\frac{B_0}{w_0}\right]-\frac{B_0}{w}\ , \tag{59a}$$

where

$$w=w_0-\alpha\theta+\tfrac{1}{2}\alpha_2\theta^2\ . \tag{59b}$$

Inverting Eq. (59b), we get (since $\alpha_2\theta^2\ll 1$)

$$\theta=-\frac{w-w_0}{\alpha}+\frac{\alpha_2}{2\alpha^2}(w-w_0)^2\ , \tag{60}$$

and, therefore,

$$\int_0^\theta w\,d\theta=\left[1+\frac{\alpha_2 w_0}{6\alpha^2}\right]\frac{w_0^2}{2\alpha}-\left[1+\frac{\alpha_2}{\alpha^2}(w_0-\tfrac{2}{3}w)\right]\frac{w^2}{2\alpha}\ . \tag{61}$$

Instead of Eq. (51), where $\alpha_2=0$, if we redefine the initial condition by the relation

$$U_{00}=\tilde{U}_{00}e^{i(1+a_2w_0/6\alpha^2)w_0^2/2\alpha}-\frac{B_0}{w_0}\ , \tag{62}$$

then Eq. (59a) becomes

$$U_0\sim\tilde{U}_{00}e^{i\{1+(\alpha_2/\alpha^2)[w_0-(2/3)w]\}w^2/2\alpha}-\frac{B_0}{w}\ . \tag{63}$$

Notice that U_0 depends on w_0 and, therefore, on τ_0. However, if $\alpha_2 w_0/\alpha^2\ll 1$, then the dependence is weak and the solution of Eq. (36) with the initial condition given by Eq. (62) is also weakly dependent on τ_0. Equation (63) indicates that as θ tends to minus infinity, $||U_0|^2-|\tilde{U}_{00}|^2|$ tends to zero, and, therefore, $\tilde{U}_{00}$ is the appropriate parameter around which the detuning factor should be expanded. Also, $w_0,\alpha,\alpha_2,\delta$ are functions of $\tilde{U}_{00}$. As before, we call $\tilde{U}_{00}$ the asymptotic initial value of U_0. From this point on, the solutions of Eqs. (28) and (29) are obtained using the initial condition computed from Eq. (62). If such an approach is not followed, each small change in the initial parameters, e.g., $(\gamma\beta_\theta)_{00}, B_{\theta 0}$, etc., would produce a different U_0 which could be either in the Fresnel or the lock-in regime, to the extent that one might get the impression that the behavior is random.

An analytic expression of $\beta_\perp^{(0)}$ on θ, above threshold, can be easily obtained assuming that $(\gamma\beta_\theta)_0$ remains almost constant. This assumption is justified by the numerical solution of either Eqs. (28) and (29) or Eq. (36). Results are shown in Fig. 9(b) for the same parameters listed in Table II, except that $\delta B_{z0}=0.4$ G. In contrast to the solutions of Eqs. (28) and (29) or Eq. (36), Eq. (40) predicts that $(\gamma\beta_\theta)_0$ initially behaves in the same manner, but gradually increases as θ (or time) increases to very large values. The exact Eq. (4) or (12) gives also an average $\gamma\beta_\theta$ that varies as in Fig. 9(b). Since $\gamma\beta_\theta$ remains constant, on the average, after the resonance has been reached, we conclude that

$$(\gamma_0+\gamma'\theta)^2-1-|U_0|^2=\text{const}\ . \tag{64}$$

If the initial value $\tilde{U}_{00}=0$, then at $\theta=\theta_0\equiv w_0/\alpha$, we have $|U_0|\approx 0$ and $\gamma=\gamma_0+\gamma'\theta_0$, and Eq. (64) leads, to zero or-

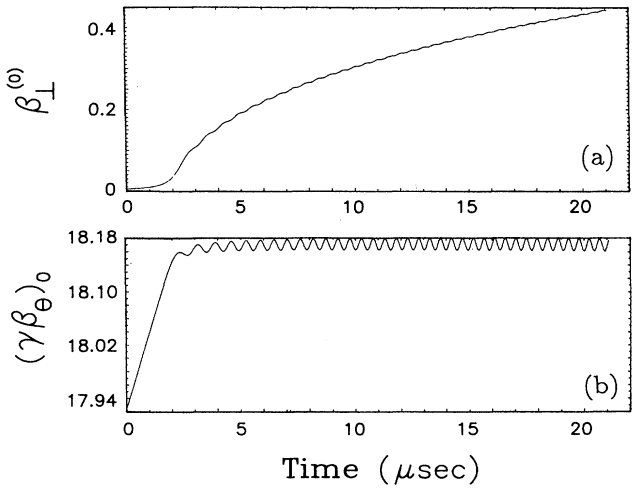

FIG. 9. Asymptotic behavior of $\beta_\perp$ and $\gamma\beta_\theta$ above the threshold (lock-in regime) for the parameters of Table II, except that $\delta B_{z0}=0.4$ G.

der in $\beta_\perp$, to the expression

$$\beta_\perp^2 \approx \frac{1+\frac{\gamma'}{2\gamma_0}(\theta+\theta_0)}{\left[1+\frac{\gamma'}{\gamma_0}\theta\right]^2}\frac{2\gamma'}{\gamma_0}(\theta-\theta_0) . \tag{65}$$

When $\gamma'\theta \ll \gamma_0$, $\beta_\perp$ is proportional to the square root of time, which is demonstrated in Fig. 9(a) and also $\beta_\perp$ is proportional to the square root of the acceleration rate γ'. In contrast, below threshold, it has been shown that $\beta_\perp$ is inversely proportional to the square root of γ'.

V. DYNAMIC STABILIZATION AND THRESHOLD LAW

There are at least three possible ways to cross a cyclotron resonance without locking into it: (a) by reducing or eliminating the field errors, (b) by accelerating fast through the resonance, and (c) by adding a small time-dependent toroidal field that provides dynamic stabilization. In effect, it will be shown that the dynamic stabilization is equivalent to increasing the acceleration rate. The effectiveness of the second stabilizing mechanism is discussed at the end of this section. Here, we analyze the effectiveness of the stabilizing toroidal field, which is assumed to be sinusoidal with amplitude $\delta B_{\theta 0}$, and period τ which is much larger than the time Δt is takes to cross the resonance. The total toroidal field is described by

$$B_{\theta 0}(t) = B_{\theta 0} + \delta B_{\theta 0} \sin\frac{2\pi(t-t_d)}{\tau} , \tag{66}$$

where t_d is the time delay. Inserting Eq. (66) into Eqs. (13b) and (19b) [with the initial value $B_{\theta 0}(0)$ in b_{00}] and linearizing the detuning factor in Eq. (36), the parameters α, α_2 become

$$\alpha = \nu_{+1}\left[\lambda_0 - \kappa_0 \frac{\delta\Omega_{\theta 0}}{\Omega_{\theta 0}(0)}\cos\left[\frac{2\pi t_d}{\tau}\right]\right] , \tag{67a}$$

$$\alpha_2 = \left[3 - \frac{(\gamma\beta_\theta)_{00}^2}{\gamma_0^2}\right]\lambda_0\alpha + \frac{r_0\delta\Omega_{\theta 0}}{(\gamma\beta_\theta)_{00}c}\kappa_0^2 \sin\left[\frac{2\pi t_d}{\tau}\right] , \tag{67b}$$

where

$$\lambda_0 = \frac{\gamma_0\gamma'}{(\gamma\beta_\theta)_{00}^2} , \tag{68a}$$

$$\kappa_0 = \frac{2\pi}{\tau}\frac{r_0}{c}\frac{\gamma_0}{(\gamma\beta_\theta)_{00}} , \tag{68b}$$

and w_0, δ, ν_{+1} are given by Eqs. (39a), (39c), and (39d). The expansion of the detuning factor in Eq. (36) is done around $\tilde{U}_{00}$ and not around the initial value U_{00}, so that all the parameters given above depend on $\tilde{U}_{00}$. For simplicity, let us assume that $t_d = 0$. If the toroidal field decreases as the resonance is being crossed, i.e., if $\delta B_{\theta 0} < 0$, then according to Eq. (67a) α becomes larger. This is equivalent to replacing γ' in α with a larger effective value. It is shown shortly that the larger the acceleration rate, the larger becomes the threshold value. Therefore a small time-dependent toroidal field with negative time derivative does provide dynamic stabilization.

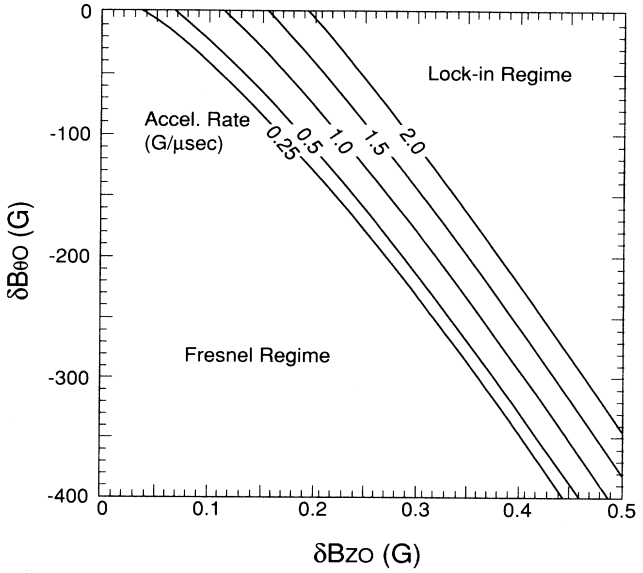

FIG. 10. Threshold law in the presence of a stabilizing time-dependent toroidal magnetic field, i.e., $\delta B_\theta = \delta B_{\theta 0}\sin(2\pi t/\tau)$ and zero initial perpendicular velocity ($\tilde{U}_{00} = 0$).

The threshold law is obtained by determining numerically the threshold value of $\hat{\epsilon}$ in the dimensionless Eq. (47) in the special case when $\hat{\tilde{U}}_{00} = 0$. Then the threshold law is expressed by the relation

$$\frac{\delta}{2\alpha^{3/2}} B_{0\text{thr}}^2 = \hat{\epsilon}_{\text{thr}}^2 \equiv 1.36 . \tag{69}$$

Figure 10 gives the threshold values of δB_{z0} as a function of $\delta B_{\theta 0}$ for different acceleration rates, when $B_{\theta 0} = 2771$ G, $\tau = 50$ μsec, and $l = 9$. The beneficial effect of a large acceleration rate or a small time-dependent toroidal field becomes obvious from this figure. Each line in the figure separates the Fresnel from the lock-in regimes for each different value of the acceleration rate.

VI. DYNAMIC BEHAVIOR WITH INITIAL PERPENDICULAR VELOCITY

When the asymptotic initial value of U_0 is not zero, the display of the dynamic behavior close to the resonance becomes more difficult, because the dynamics depend on the initial phase as well as on the initial amplitude of $\tilde{U}_0$. The results are conveniently presented as contour plots (i.e., the resonance diagrams) of the final $\beta_\perp \equiv |U_0|/\gamma$ in the $\beta_\perp^{(0)}(0), \varphi_0$ plane, where $\beta_\perp^{(0)}(0)$ and φ_0 are the amplitude and phase of the asymptotic initial value $\tilde{U}_{00}/\gamma_0$. The rest of the parameters, including the interval of integration over θ or time, are kept constant. Since the final $\beta_\perp$ becomes large in the lock-in regime while it is bounded in the Fresnel regime, the contours are very dense at the boundary between the two regions.

Figure 11 shows the two regimes for the parameters listed in Table IV. Although the results shown in Fig. 11

TABLE IV. Parameters of the run shown in Figs. 11 and 12.

Parameter	Value
Torus major radius r_0	100 cm
Toroidal magnetic field $B_{\theta 0}$	2771 G
Initial generalized mismatch $\Delta_0+0.5\|V_0\|^2$	0.0
Field index n	0.5
Rate of change of vertical field $\dot{B}_{z0}$	2,4 G/μsec
Resonance mode l	9
Amplitude of VF error δB_{z0}	0.195,0.3 G
Constant phase of VF error θ_0	0.0
Gradient of VF error K_{r0}	0.0
Amplitude of stabilizing toroidal field $\delta B_{\theta 0}$	0,−200 G
Period of stabilizing toroidal field τ	70 μsec
Time delay of stabilizing toroidal field t_d	0.0 μsec
Initial normalized toroidal momentum $\gamma\beta_\theta$	17.922
Initial normalized radial bounce displacement ξ_{0x}	0.0,0.003,−0.003
Initial normalized vertical bounce displacement ξ_{0z}	0.0
Integration time t_f	8 μsec

have been obtained by integrating Eqs. (28) and (29), Eq. (36) or (40) gives the same results, provided that there is negligible bounce motion. In Fig. 11(a), δB_{z0} has been chosen equal to 0.195 G, which is very close to the threshold value when $\beta_\perp^{(0)}(0)$. By increasing the field error amplitude from 0.195 to 0.3 G, the lock-in regime dominates for small initial $\beta_\perp^{(0)}(0)$ for the entire range of initial phase angles as shown in Fig. 11(b). By turning on the stabilizing field, the Fresnel region increases at the expense of the lock-in region. Results are shown in Fig. 11(c) for $\delta B_{z0}=0.195$ G and $\delta B_{\theta 0}=-200$ G. This figure should be compared with Fig. 11(a) that has the same field error amplitude but not stabilizing field. Finally, in Fig. 11(d) the acceleration rate has been increased from

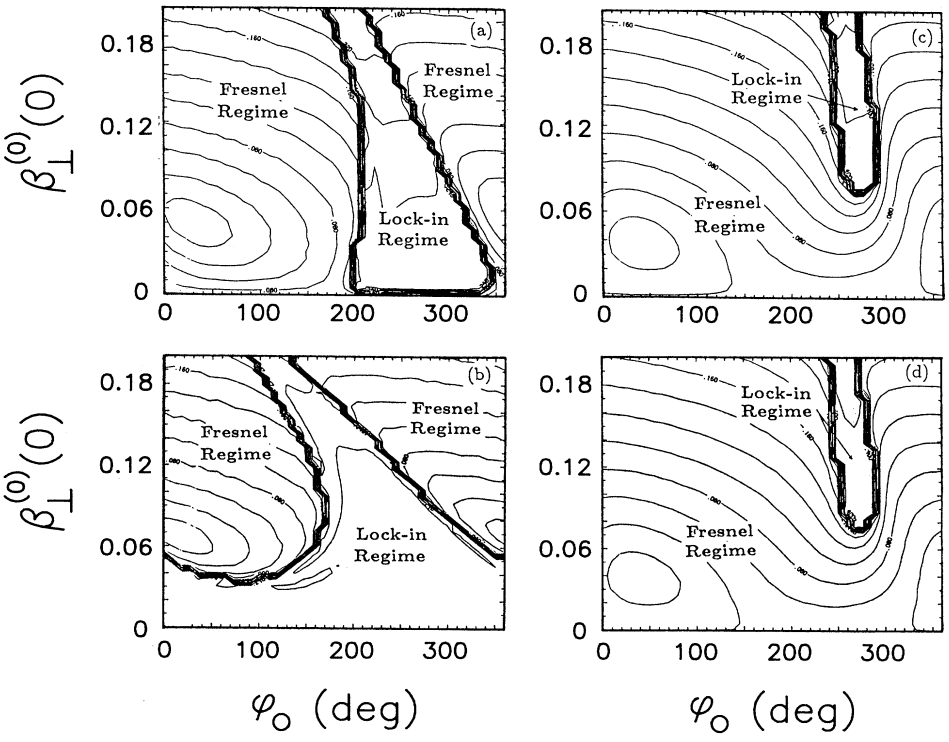

FIG. 11. Resonance diagrams, i.e., contour plots of the final $\beta_\perp$, when the initial amplitude and phase of the normalized perpendicular velocity $\tilde{U}_{00}/\gamma_0$ are not zero, for the parameters in Table IV, and in (a) $\delta B_{z0}=0.195$ G, $\delta B_{\theta 0}=0.0$ G, $\dot{B}_{z0}=2$ G/μsec; (b) $\delta B_{z0}=0.3$ G, $\delta B_{\theta 0}=0.0$, $\dot{B}_{z0}=2$ G/μsec; (c) $\delta B_{z0}=0.195$ G, $\delta B_{\theta 0}=-200$ G, $\tau=70$ μsec, $\dot{B}_{z0}=2$ G/μsec; (d) $\delta B_{z0}=0.195$ G, $\delta B_{\theta 0}=0.0$ G, $\dot{B}_{z0}=4$ G/μsec.

$\dot{B}_{z0}=2$ to 4 G/μsec, while $\delta B_{z0}=0.195$ G and $\delta B_{\theta 0}=0$. Again, comparison of Fig. 11(d) with Fig. 11(a) shows that the Fresnel region has increased at the expense of the lock-in region. When the electrons in the ring are uniformly distributed over the initial phase angle, the resonance diagrams give, for each initial $\beta_{\perp}^{(0)}(0)$, the percentage of the ring that crosses the resonance and the percentage that locks into it.

In all the results presented so far, the equilibrium position of the bounce motion was located at the origin of the coordinate system [i.e., $\Delta_{00}+|\tilde{U}_{00}|^2/2(\gamma\beta_\theta)_{00}^2=0$] and the amplitude of the bounce motion was selected negligibly small (since the initial $\xi_0=0$). If the equilibrium position is chosen off the origin [i.e., $\Delta_{00}+|\tilde{U}_{00}|^2/2(\gamma\beta_\theta)_{00}^2\neq 0$], and the amplitude of the bounce motion is negligibly small, by judicially choosing ξ_{00}, the resonance diagrams remain the same for the same set of parameters. When $\Delta_{00}+|\tilde{U}_{00}|^2/2(\gamma\beta_\theta)_{00}^2\neq 0$, and in the special case of a field index $n=\frac{1}{2}$, the parameters γ' and r_0/c in Eqs. (68a) and (68b) should be replaced by $(1+\Delta_{10})\gamma'$ and $(1+\Delta_{10})r_0/c$, respectively, where $\Delta_{10}=[\Delta_{00}+|\tilde{U}_{00}|^2/2(\gamma\beta_\theta)_{00}^2]/K_{100}$. Also, the initial bounce position must be equal to $\xi_{00}=\Delta_{10}$, to have bounce motion with negligible amplitude. Finally, the term

$$(\nu_- -2b_0\zeta_0)\left[\Delta_0+\frac{1}{2}\frac{|U_0|^2}{(\gamma\beta_\theta)_0^2}\right]\Big/K_{10}$$

should be added to the detuning factor in Eq. (36), and, therefore, the term $(\nu_{-0}-2b_{00}\zeta_{00})\Delta_{10}$ should be added to w_0 in Eq. (39a), where ν_{-0} is the initial value of the bounce frequency.

When there is a small bounce motion superimposed to the cyclotron motion there is a modest change of the resonance diagrams. This becomes apparent by comparing Fig. 11(a) with Fig. 12. These figures have been obtained from Eqs. (28) and (29) with the same parameters, except for the initial bounce position. In Fig. 11(a), the initial position of the bounce motion is at the origin, while in Fig. 12(a), it is at (0.30 cm, 0.0 cm) and in Fig. 12(b) it is at (−0.30 cm, 0.0 cm). In the latter two cases, the amplitude of the bounce motion is 0.30 cm.

VII. MULTIPLE CROSSING OF A RESONANCE

When a small toroidal field with sinusoidal time dependence is added to the main toroidal field $B_{\theta 0}$, the detuning factor may become zero more than once, as time evolves, for the *same* resonance mode l. This is defined as a multiple crossing of the resonance mode l. Results are shown in Fig. 13. These results have been obtained from Eqs. (28) and (29) for the parameters listed in Table V and $\delta B_{z0}=0.35$ G. Figure 13(a) shows that the detuning factor w becomes zero five times and a Fresnel jump occurs each time the resonance mode l is crossed. It is not necessary that all the crossings have a Fresnel jump. A lock into the resonance could occur at some crossing if

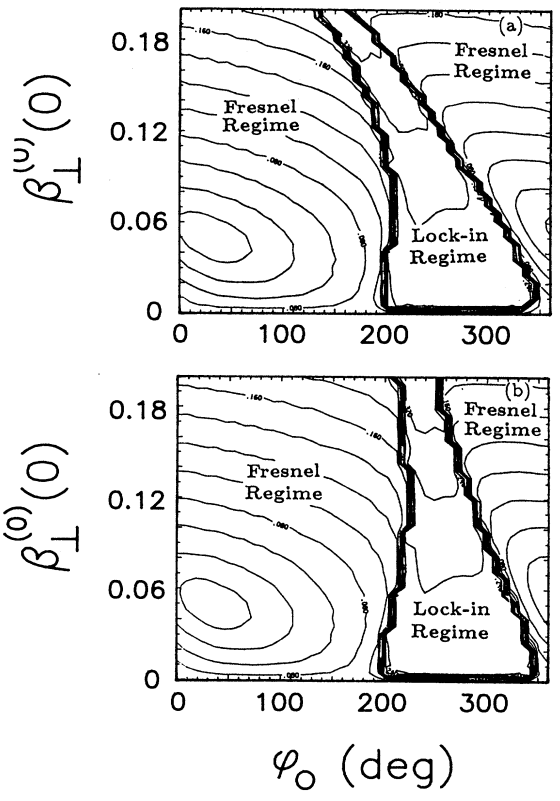

FIG. 12. Resonance diagrams for the same parameters as in Fig. 11(a), except that the radius of the bounce motion is 0.3 cm in both (a) and in (b) and in (a) the initial position of the bounce motion, i.e., $\xi_{00}=(0.3$ cm, 0.0 cm); in (b) $\xi_{00}=(-0.3$ cm, 0.0 cm).

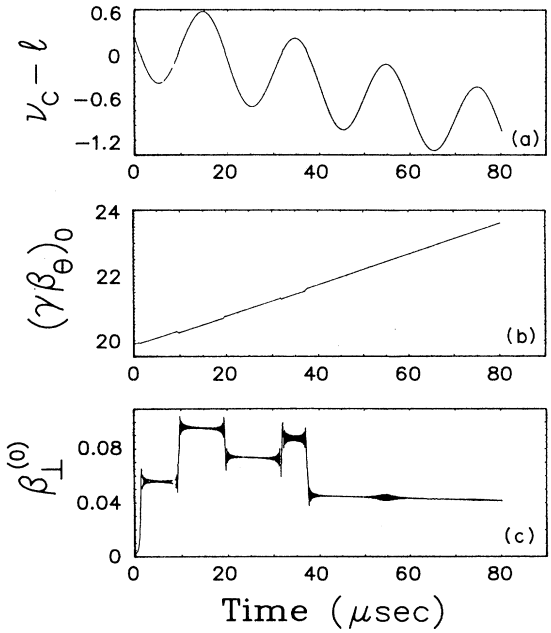

FIG. 13. $\nu_c - l$, $\gamma\beta_\theta$, and $\beta_\perp$ vs time during a multiple crossing of the resonance $l=8$, obtained from the slow equations of motion [Eqs. (28) and (29)], for the parameters of Table V, and $\delta B_{z0}=0.35$ G.

TABLE V. Parameters of the run shown in Fig. 7.

Parameter	Value
Torus major radius r_0	100 cm
Toroidal magnetic field $B_{\theta 0}$	2771 G
Initial generalized mismatch Δ_0	0.0
Field index n	0.5
Rate of change of vertical field $\dot{B}_{z0}$	0.8 G/μsec
Resonance mode l	8
Amplitude of VF error δB_{z0}	0.35,1.0 G
Constant phase of VF error θ_0	0.0
Gradient of VF error K_{r0}	0.0
Amplitude of stabilizing toroidal field $\delta B_{\theta 0}$	-200 G
Period of stabilizing toroidal field τ	20 μsec
Time delay of stabilizing toroidal field t_d	0.0 μsec
Initial normalized toroidal momentum $\gamma\beta_\theta$	19.875
Initial normalized vertical velocity $\beta_\perp$	0.0
Initial phase of vertical velocity φ_0	0.0
Initial normalized radial bounce displacement ξ_{0x}	0.0
Initial normalized vertical bounce displacement ξ_{0z}	0.0
Integration time t_f	80 μsec

the asymptotic initial velocity is in the lock-in regime of the resonance diagram. As a rule, the detuning factor follows the time-dependent toroidal field. Figure 13(b) shows that when all the crossings are in the Fresnel regime, $\gamma\beta_\theta$ follows γ between crossings, while Fig. 13(c) shows that there are five Fresnel jumps in $\beta_\perp$. In contrast, when the ring locks into the resonance, then $\gamma\beta_\theta$ follows the time-dependent toroidal field while w remains very small. This is shown in Fig. 14, obtained by integrating Eqs. (28) and (29), for the parameters listed in Table V and $\delta B_{z0}=1.0$ G. According to Fig. 14(a) the first crossing occurs at 1 μsec and the ring locks into the resonance up to approximately 10 μsec. As long as it remains locked, $w\approx 0$, while $\gamma\beta_\theta$ follows the time varying toroidal field [Fig. 14(b)]. Figure 14(c) shows that just before 10 μsec, $\beta_\perp$ decreases to zero, while $\gamma\beta_\theta$ increases at a faster rate than γ. Since at this time $(\gamma\beta_\perp)^2=\gamma^2-1-(\gamma\beta_\theta)^2\approx 0$, a continuously rising $\gamma\beta_\theta$ would require a negative $(\gamma\beta_\perp)^2$, which is an unphysical situation. Thus the ring unlocks from the resonance. The same cycle is repeated up to 45 μsec, when $\beta_\perp$, due to

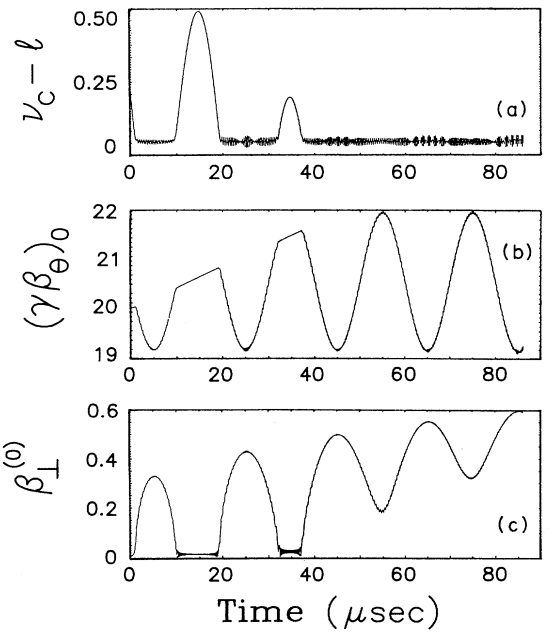

FIG. 14. ν_c-l, $\gamma\beta_\theta$, and $\beta_\perp$ vs time during a multiple crossing of the resonance $l=8$ under the same conditions as in Fig. 13, except that $\delta B_{z0}=1.0$ G.

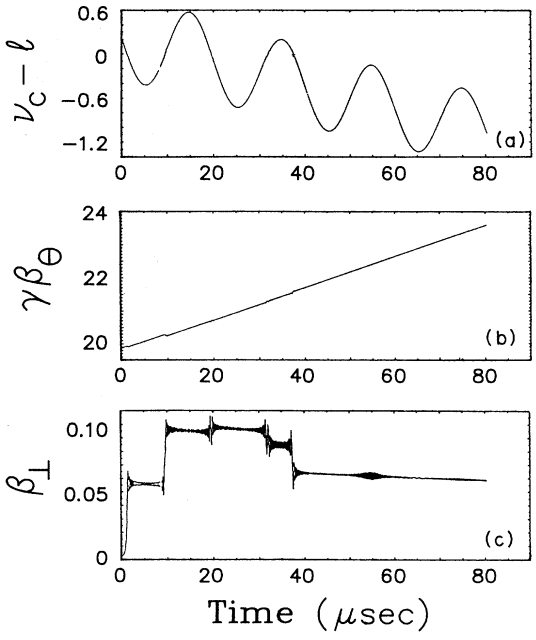

FIG. 15. ν_c-l, $\gamma\beta_\theta$, and $\beta_\perp$ vs time during a multiple crossing of the same resonance $l=8$, under the same conditions as in Fig. 13, but obtained by integrating the exact equations of motion [Eq. (4)].

the rise of its average value, cannot become zero. After this time, $\gamma\beta_\theta$ remains locked to the sinusoidal variation of the field, while w remains almost zero. Therefore the next resonance mode $l+1$ is never reached, in spite of the fact that γ keeps increasing. The energy is transferred to $\gamma\beta_\perp$ rather than $\gamma\beta_\theta$. The exact Eq. (4) or (5) or the nonlinear slow Eq. (36), give identical results to those obtained from Eqs. (28) and (29) which are shown in Fig. 14. However, this is not the case with Fig. 13. Results from the integration of the exact Eq. (4) for the parameters listed in Table V and $\delta B_{z0}=0.35$ G are shown in Fig. 15. The detuning factor and $\gamma\beta_\theta$ in Fig. 15(a) and 15(b) are very similar to the results shown in Figs. 13(a) and 13(b). However, the transverse velocity in Fig. 15(c) is similar to that of Fig. 13(c) until the third crossing occurs at 19 μsec. The difference is due to the fact that the slow Eqs. (28) and (29) are approximate, and the phase of $\beta_\perp$ computed from the exact and the slow equations becomes gradually different for long times. Therefore, for long times, when many resonances are to be crossed or multiple crossing occurs, the exact Eq. (4) should be used. The slow equations provide a valuable insight in the dynamic behavior close to a particular resonance, but are not reliable over long periods of time.

VIII. SUMMARY AND CONCLUSIONS

Magnetic-field errors excite resonances that the electron ring must cross during acceleration. In the presence of a VF error, there is a threshold value of the field error amplitude that separates two distinct regimes. Below threshold (Fresnel regime) and for zero initial $\tilde{U}_{00}$, the perpendicular velocity increases by a finite amount as the resonance is crossed. The increase as well as the time it takes to cross the resonance are inversely proportional to the square root of the acceleration rate. Above threshold (lock-in regime), the perpendicular velocity is proportional to the square root of the acceleration rate and increases with the square root of time, while $\gamma\beta_\theta$ remains on the average constant, and the detuning factor remains extremely small. Therefore the ring locks into the resonance. The dynamic behavior without acceleration is entirely different even at exact resonance. The perpendicular velocity is proportional to time initially, but, due to the nonlinearities in the equations of motion, it reaches a maximum, then it decreases to zero and repeats periodically the same cycle. Therefore it is bounded.

The threshold is predicted by the slow equations of motion that have been derived by averaging out the fast cyclotron motion. The origin is the nonlinear dependence of $\gamma\beta_\theta$ on the perpendicular velocity and the fact that the cyclotron frequency is inversely proportional to $\gamma\beta_\theta$. By the appropriate choice of the initial conditions it was shown that the solutions of the slow or the exact equations of motion could be made weakly dependent on the initial time interval from the resonance. Possible ways to increase the threshold have been discussed. It has been shown, that the threshold value of the VF error amplitude is proportional to the $\frac{3}{4}$ power of the acceleration rate. Dynamic stabilization, i.e., the addition of a small time-dependent field to the main toroidal field, also provides an effective increment to the acceleration rate, if it has a negative time derivative, and, therefore, increases the threshold. When the initial perpendicular velocity is not zero, the dynamic behavior has been presented by means of the resonance diagrams. These diagrams predict that a small bounce motion has only a modest effect on the Fresnel and lock-in regimes. Finally, the multiple crossing of the same resonance has been analyzed in the presence of dynamic stabilization and we have concluded that for long periods of time the exact equations of motion should be used.

Following the successful demonstration of acceleration in the NRL device, a concerted effort was made to locate and eliminate or reduce the various field disturbances that may excite the cyclotron resonance. Reduction in many of these field errors, together with the operation of higher toroidal and strong focusing fields led to beam energies in excess of 20 MeV, while the trapped current was above 1 kA.

In addition, three different cyclotron resonance stabilization techniques were tested in the NRL modified batatron: enhancement of the acceleration rate, dynamic stabilization or tune jumping, and avoidance of the resonance.

The damage done to the beam at each resonance depends on the speed with which the resonance is crossed. By enhancing the acceleration rate the resonance is crossed faster and thus the damage inflicted to the beam is reduced. To achieve higher acceleration rate, the vertical field coils were divided into two halves with midplane symmetry and powered in parallel. The experimental results show a striking reduction of the beam losses at $l=12$, 11, and 10, when the acceleration rate increased from 0.69 to 1.93 G/μsec.

The crossing of the resonance can be also speeded up by modulating the toroidal magnetic field with a rapidly varying ripple. This is the dynamic stabilization or tune jumping technique and requires a carefully tailored pulse to be effective over many resonances. These results have been reported [10] previously and in general they are in agreement with the predictions of Sec. V and extensive computer calculations.

It is apparent from the resonance condition that when $B_{\theta 0}/B_{z0}=\text{const}\neq\text{integer}$, the cyclotron resonance is not excited. To test this prediction, a linearly rising toroidal field ramp ΔB_θ was superimposed on the main toroidal field. During the rise time of the ramp (~ 100 μsec), the ratio $B_{\theta 0}+\Delta B_\theta/B_{z0}\approx\text{const}\neq\text{integer}$. The experimental results indicate that during this time period the beam losses are completely suppressed. Although very powerful, the resonance avoidance technique by keeping the ratio $B_{\theta 0}/B_{z0}=\text{const}\neq\text{integer}$ is not practical because to be effective over the entire spectrum of l requires very high toroidal field. Among the three stabilization techniques tested, acceleration of the beam at a higher acceleration rate appears to have the highest practical potential.

ACKNOWLEDGMENT

This work was supported by the U.S. Office of Naval Research and by SPAWAR.

*Also at Science Applications International Corporation, McLean, VA 22102.

†Also at SFA, Inc., Landover, MD 20785.

[1] C. A. Kapetanakos, L. K. Len, T. Smith, J. Golden, K. Smith, S. J. Marsh, D. Dialetis, J. Mathew, P. Loschialpo, and J. H. Chang, Phys. Rev. Lett. **64**, 2374 (1990).

[2] C. A. Kapetanakos, L. K. Len, T. Smith, D. Dialetis, S. J. Marsch, P. Loschialpo, J. Golden, J. Mathew, and J. H. Chang, Phys. Fluids B **3**, 2396 (1991).

[3] L. K. Len, T. Smith, P. Loschialpo, J. Mathew, S. J. Marsch, D. Dialetis, J. Golden, J. H. Chang, and C. A. Kapetanakos, Proc. SPIE, Intense Microwave and Particle Beams III **1629**, 521 (1992).

[4] C. A. Kapetanakos, S. J. Marsh, and D. Dialetis, Phys. Rev. Lett. **61**, 86 (1988).

[5] D. Chernin and P. Sprangle, Part. Accel. **12**, 101 (1982).

[6] D. C. DePackh, NRL Report No. 4608, 1955 (unpublished).

[7] C. W. Roberson, A. Mondelli, and D. Chernin, Part. Accel. **17**, 79 (1985).

[8] N. N. Bogoliubov and Y. A. Mitropolsky, *Asymptotic Methods in the Theory of Nonlinear Oscillations* (Hindustan, Delhi, 1961).

[9] I. S. Gradshteyn and I. M. Ryzhik, *Table of Integrals, Series and Products* (Academic, New York, 1980), Sec. 3.145, Eq. 2.

[10] C. A. Kapetanakos, L. K. Len, T. Smith, P. Loschialpo, J. Mathew, S. J. Marsh, D. Dialetis, J. Golden, and J. H. Chang, NRL Memo Report No. 6988, 1992 (unpublished).